VIBRATIONAL ANALYSIS OF THE STRUCTURE OF GRAMICIDIN A.

I. Normal Mode Analysis

VAMAN M. NAIK AND S. KRIMM
Biophysics Research Division, University of Michigan, Ann Arbor, Michigan 48109

ABSTRACT Normal mode frequencies have been calculated for single-stranded $\beta^{4.4}$ and $\beta^{6.3}$ and for double-stranded $\uparrow\downarrow\beta^{5.6}$, $\uparrow\downarrow\beta^{7.2}$, $\uparrow\uparrow\beta^{5.6}$, and $\uparrow\uparrow\beta^{7.2}$ helices that are possible models for the structure of gramicidin A. The force field used in the calculations is one that reproduces the frequencies of model polypeptide chain structures to about ± 5 cm^{-1}, and is therefore expected to provide meaningful distinctions between these conformations. The calculations predict significant differences in the infrared and Raman spectra of these β-helices, suggesting that they should be identifiable from their spectra (which is shown in the following paper to be the case). The most sensitive region is that of the amide I frequencies, where the predicted patterns of intense infrared mode, infrared splittings, and intense Raman mode provide a characteristic identification of each of the above structures.

INTRODUCTION

Gramicidin A (GA) is a linear alternating L,D pentadecapeptide that facilitates the passive transport of alkali metal ions and water molecules across biological membranes and synthetic lipid bilayers (Haydon and Hladky, 1972; Krasne et al., 1971). A number of studies show that the dimeric form of this molecule performs the transmembrane channel function (Urry et al., 1971; Bamberg and Läuger, 1973; Zingsheim and Neher, 1974; Kolb et al., 1975; Veatch et al., 1975; Apell et al., 1977; Veatch and Stryer, 1977). Since this represents a basic property of membranes, it is clearly of importance to know the nature of the mechanism involved in such transport. Knowledge of the three-dimensional structure of the GA molecule is obviously a prerequisite to such understanding.

Stereochemical and conformational energy analyses of L,D-peptides (Urry, 1971, 1972; Hesselink and Scheraga, 1972; Ramachandran and Chandrasekharan, 1972) showed that, although an α-helix is a possible conformation, GA probably adopts a single-stranded, so-called β-helix, conformation, with 6.3 L plus D residues per turn being the most likely structure for the conducting species (Urry, 1971). Studies of the activity of a malonyl dimer of GA (Urry et al., 1971) indicated that the active species is a head-to-head (formyl end-to-formyl end) dimer of such $\beta^{6.3}$-helices. However, on the basis of chemical and spectroscopic studies in organic solvents, it was suggested that GA could also exist as double-stranded helices, with parallel or antiparallel chains (Veatch et al., 1974). Conformational energy calculations (Prasad and Chandrasekharan, 1977; Colonna-Cesari et al., 1977; Popov and Lipkind, 1979) have shown that such structures are stable, although the almost identical energies of single- and double-stranded helices have provided no basis for clearly preferring one over the other.

A variety of experimental studies have been undertaken to establish the actual structure of GA in particular systems. X-ray diffraction of native and ion-bound GA (Koeppe et al., 1978; Koeppe et al., 1979), and low-resolution Fourier maps from neutron diffraction (Koeppe and Schoenborn, 1984), have provided information on the size and shape of the molecule in the crystalline state. A synthetic oligomer, t-Boc-(L-Val-D-Val)$_4$-OCH$_3$, was found to exist as a left-handed antiparallel-chain double-stranded helix (designated $\uparrow\downarrow\beta^{5.6}$) by single crystal x-ray analysis (Benedetti et al., 1979). And poly(γ-benzyl-L,D-glutamate) has been shown by x-ray and electron diffraction to adopt both single-stranded (Heitz et al., 1975) and double-stranded (Lotz et al., 1976) structures. NMR studies have been very fruitful. Using spin labels to determine the accessibility of the COOH- or NH$_2$-terminus of GA, it was found (Weinstein et al., 1979, 1980) that the COOH-terminus was the accessible one at the surface of a vesicle, indicating the existence of a head-to-head dimer in phospholipid vesicles. By incorporating ^{13}C into various L-residue carbonyl carbons and measuring thallium ion-induced chemical shifts, Urry et al. (1983*a*) were able to

This is paper number 33 in a series on "Vibrational Analysis of Peptides, Polypeptides, and Proteins", of which Sengupta and Krimm (1985) is paper number 32.

Dr. Naik's present address is the Department of Physics, Northeastern University, Boston, MA 02115

show that the transmembrane channel is a head-to-head dimer formed from left-handed $\beta^{6.3}$-helices. In dioxane solution, however, NMR studies indicate (Arseniev et al., 1984) that GA has a double-stranded $\uparrow\downarrow\beta^{5.6}$ structure. Circular dichroism, while not enabling the determination of the specific three-dimensional structure, has been consistently useful in identifying the presence of a particular species in a given environment (Veatch et al., 1974; Urry et al., 1979; Wallace et al., 1981; Urry et al., 1983*a*, *b*; Wallace, 1983, 1984).

Vibrational spectroscopy, which is inherently capable of defining three-dimensional structure and can be used for a variety of physical states, has had limited use in the detailed analysis of the structure of GA. In an early infrared study (Veatch et al., 1974) the presence of a splitting in the amide I mode was used to infer, by analogy with β-sheet structures, the existence of an antiparallel-chain double-stranded structure for GA. The first Raman study of GA (Rothschild and Stanley, 1974) observed spectral differences between GA in the solid state and in DMSO, but no convincing structural conclusions could be drawn. In subsequent infrared studies (Iqbal and Weidekamm, 1979, 1980) the amide I splittings were analyzed in greater detail, but observed Raman amide I bands (Iqbal and Weidekamm, 1980) could not be reconciled with the infrared. More problematic, however, was the fact that in these studies, as well as in a calculation using specific b-helix structures (Sychev et al., 1980), the questionable assumption was made that all amide I eigenvectors participating in transition dipole coupling (Krimm and Abe, 1972) could be taken to be equal. In addition, the nature of the calculation (Sychev et al., 1980) required that the unperturbed amide I frequency be obtained by empirical fitting of observed data. These results have been the basis for proposals (Sychev et al., 1980; Ovchinnikov and Ivanov, 1982) that hybrid helices are present under certain conditions, including the existence of "hairpin" turns (Sychev and Ivanov, 1982). Infrared dichroism has been used to study the orientation of GA in lipid vesicles (Nabedryk et al., 1982), leading to the conclusion that the axis of the helical GA molecule is essentially perpendicular to the plane of the membrane. In another infrared study of GA in vesicles (Urry et al., 1983*b*) it was claimed that the amide I frequency could not distinguish between single- and double-stranded structures. However, in this as well as in some other studies (Sychev and Ivanov, 1982; Ovchinnikov and Ivanov, 1982), D_2O was used in place of H_2O, and neglect of the effect of *N*-deuteration on the amide I frequency leaves these interpretations questionable.

The only rigorous spectroscopic basis for obtaining definitive information on the three-dimensional structure of polypeptide molecules is through the use of normal mode analysis to predict the vibrational frequencies expected for a given conformation. The systematic refinement of a vibrational force field for polypeptides and its application to a variety of molecules (Krimm, 1983) has demonstrated the power of this approach. We have used this method to study the vibrational spectra of GA, and have been able to reach specific conclusions about its structure in the crystalline and vesicle-bound states. Some preliminary results have already been published (Naik and Krimm, 1984*a*, *b*). Here we give the detailed results of our normal mode calculations; in the following paper (Naik and Krimm, 1986) we present an analysis of the vibrational spectra of GA in various states in terms of its structure.

NORMAL MODE CALCULATIONS

Structures

The single- and double-stranded β-helices can be designated by the symbol β^m, where m is the total number of residues (L plus D) per turn. Various values of m are possible, consistent with a satisfactory pattern of hydrogen bonding, but only certain ones are compatible with molecular lengths that are expected to span the membrane (Urry, 1972) or with dimer lengths of 25–35 Å obtained from crystallographic studies (Koeppe et al., 1978, 1979). We have restricted our normal mode calculations to such structures, which are the $\beta^{4.4}$ and $\beta^{6.3}$ single-stranded helices and the $\beta^{5.6}$ and $\beta^{7.2}$, both antiparallel-chain ($\uparrow\downarrow$) and parallel-chain ($\uparrow\uparrow$), double-stranded helices.

Coordinates of the backbone atoms of the $\beta^{4.4}$-helix were obtained from Lotz et al. (1976), while those for the $\beta^{6.3}$-helix were kindly provided by D. W. Urry. The parameters of such helices are given in Table I. We also include those of a goniomeric $\beta^{6.3}$-helix (Colonna-Cesari et al., 1977), $\beta_G^{6.3}$, whose normal modes were also computed to determine the effect of such conformational changes on the frequencies. (The $\beta_G^{6.3}$-helix can be thought of as derived from the $\beta^{6.3}$-helix by interchanging CO and NH groups and reversing the order of the dihedral angles.) In both cases right-handed helices were used, even though the $\beta^{6.3}$-helix of GA is thought to be left-handed (Urry et al., 1983). Conformational energy calculations (Venkatachalam and Urry, 1983) show that the backbone torsion angles of both kinds of helices are essentially identical, and that the lower energy of the left-handed structure is due to side chain and dimer interactions. Since in our calculations the side chain is represented by a point mass and we will be interested mainly in amide (i.e., backbone) vibrations, use of a right-handed helical structure presents no problems. ORTEP drawings of the $\beta^{4.4}$- and $\beta^{6.3}$-helices are given in Figs. 1 and 2, respectively. It should be noted that the hydrogen bonds in single-stranded L,D β-helices are of two types: type A, corresponding to $NH(D_3)\rightarrow OC(D_1)$ for $\beta^{4.4}$ and $NH(D_4)\rightarrow OC(D_1)$ for $\beta^{6.3}$; and type B, corresponding to $NH(L_1)\rightarrow OC(L_3)$ for $\beta^{4.4}$ and $NH(L_1)\rightarrow OC(L_4)$ for $\beta^{6.3}$.

Coordinates for the right-handed $\uparrow\downarrow\beta^{5.6}$- and $\uparrow\downarrow\beta^{7.2}$-helices were obtained from Lotz et al. (1976); those for the $\uparrow\uparrow\beta^{5.6}$- and $\uparrow\uparrow\beta^{7.2}$-helices were kindly provided by B. Lotz. The parameters of these helices are given in Table I, and

TABLE I
PARAMETERS OF β-HELICES

Helix	n*	h‡	ϕ_L§	ψ_L§	ϕ_D§	ψ_D§	Hydrogen Bonds		
							r(N· · ·O)‖	r(H · · · O)‖	θ¶
$\beta^{4.4}$	2.20	2.33	− 84.0	100.8	136.1	− 95.0	A**:2.76	1.81	15.2
							B**:2.85	1.93	17.7
$\beta^{6.3}$	3.13	1.53	−104.0	118.0	144.0	−132.0	A**:2.88	2.06	28.7
							B**:2.78	1.87	19.8
$\beta_G^{6.3}$‡‡	3.14	1.59	−128.7	134.7	132.6	−109.4	A**:3.00	2.07	16.8
							B**:2.95	2.00	14.0
$\uparrow\downarrow\beta^{5.6}$	2.80	4.02	−116.0	141.1	159.2	−102.9	2.76	1.83	16.8
$\uparrow\downarrow\beta^{7.2}$	3.60	2.95	−127.2	145.8	154.0	−126.4	2.90	1.92	10.5
$\uparrow\uparrow\beta^{5.6}$	2.80	4.02	133.4	− 93.0	−121.6	166.1	A**:3.09	2.20	22.3
							B**:2.56	1.88	38.5
$\uparrow\uparrow\beta^{7.2}$	3.60	2.97	135.1	−106.0	−144.4	166.4	A**:3.31	2.50	30.3
							B**:3.08	2.34	35.9

*Number of L, D units per turn of the helix.
‡Projection, in angstrom, per L, D unit on the helix axis.
§Dihedral angle, in degrees.
‖Hydrogen bond distance, in angstrom.
¶Angle between NH and N· · ·O, in degrees.
**A: D′→D hydrogen bond; B: L→L′ hydrogen bond.
‡‡Goniomeric structure (Colonna-Cesari et al., 1977).

ORTEP drawings of the antiparallel-chain helices are given in Figs. 3 and 4 (the parallel-chain helices are very similar in appearance). For the antiparallel-chain structures, all of the hydrogen bonds are equivalent to a first approximation by virtue of a local dyad perpendicular to the helix axis (we neglect small differences between the $L_k \rightarrow D_l$ and $L_l \rightarrow D_k$ hydrogen bonds for $\uparrow\downarrow\beta^{5.6}$). For the parallel-chain structures, the bonds are of the A and B types, as in the single-stranded helices.

Two additional structural considerations need to be noted. First, although calculations were done on infinite helical structures, this is not a serious problem in terms of end effects in GA: a study of the variation in the density of states of the α-helix with chain length (V. K. Datye and S. Krimm, manuscript submitted for publication) shows that the high frequency vibrational modes of a pentadecapeptide are essentially identical to those of an infinite helix. Second, in the case of the head-to-head dimer of single-stranded helices, the junction is expected to contain six hydrogen bonds between antiparallel-oriented terminal peptide groups of the two monomers (Venkatachalam and

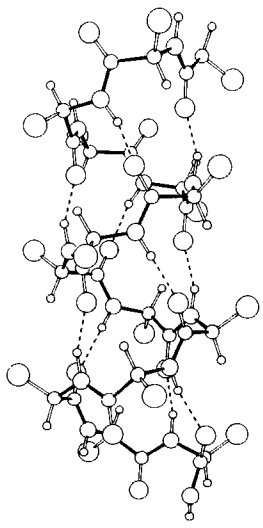

FIGURE 1 ORTEP drawing of $\beta^{4.4}$ structure.

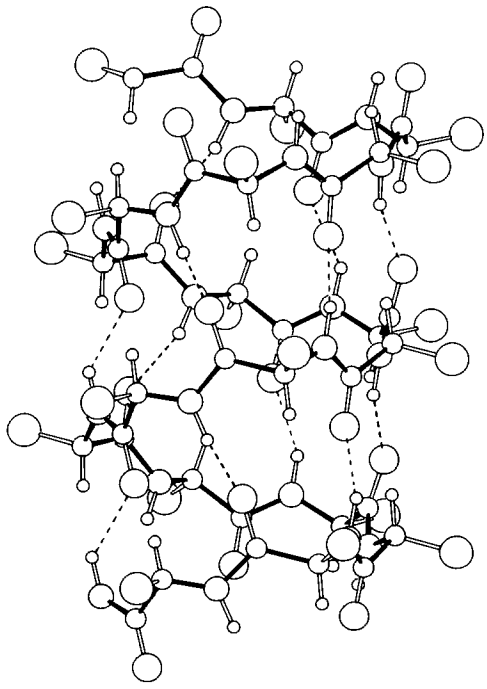

FIGURE 2 ORTEP drawing of $\beta^{6.3}$ structure.

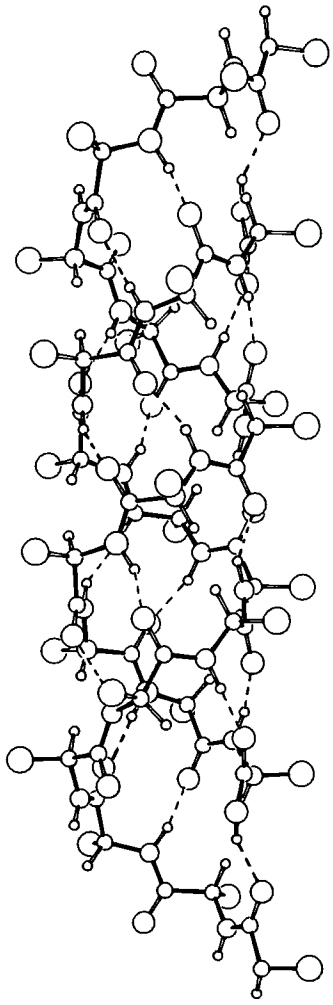

FIGURE 3 ORTEP drawing of $\uparrow\downarrow\beta^{5,6}$ structure.

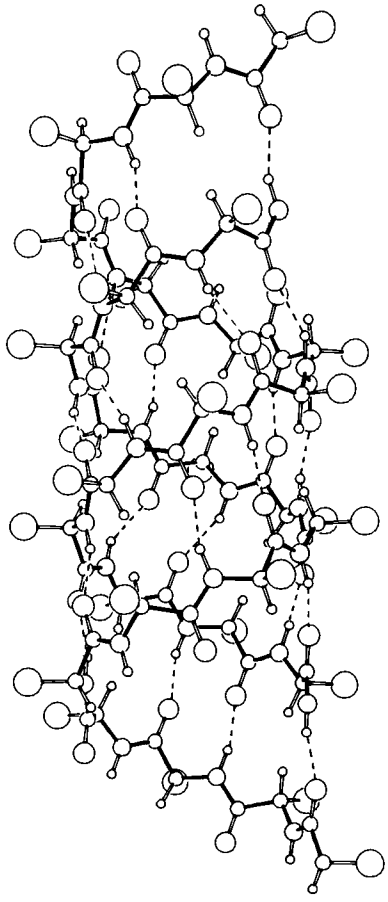

FIGURE 4 ORTEP drawing of $\uparrow\downarrow\beta^{7,2}$ structure.

Urry, 1983). It might be thought that this would significantly modify the predictions based on a single helix, but this is not the case. The high frequency modes of the helix, and therefore the effects of transition dipole coupling on the frequencies, are determined primarily by the structure, symmetry, and strong interactions within the helix, and are only slightly affected by the few weak external hydrogen bonds made by the terminal peptide groups. At most, these hydrogen bonds, by coupling the modes of the two monomers, could give rise to small (and probably unobservable) splittings in the modes of the single helix.

Force Fields

A normal mode calculation including all atoms in the side chains is not necessary for our purposes, since it would not provide significant additional information about the conformation of the backbone, to which the amide modes are primarily sensitive. We have therefore approximated the structures by replacing the side chain by a point mass equal to CH_3 at the C^β atom. The force field was one developed for this approximation.

A systematic refinement of a vibrational force field for the polypeptide chain has produced a set of force constants that can reproduce over 500 frequencies of standard structures to about ± 5 cm^{-1} (Krimm, 1983). This force field has been applied successfully to vibrational analyses of polypeptide conformations in a large number of cases (Sengupta and Krimm, 1985), and it can therefore be expected to have good predictive capability in the present application. Since the β-helical structures have local chain conformations similar to those of β-sheets, we have used a β force field in the calculation. This originated from a detailed force field for β-poly(L-alanine) (Dwivedi and Krimm, 1982*a*), which was then further refined slightly for the approximation that the CH_3 group is replaced by an equivalent mass (Dwivedi and Krimm, 1984*a*). This force field gives frequencies and potential energy distributions for the non-CH_3 modes very close to those of the detailed calculation.

Since the above force fields treat the hydrogen bond explicitly, it is necessary to modify hydrogen-bond–associated force constants so that they are consistent with the hydrogen bond geometry of the β-helical structures.

There is at present no analytical way to do this within the framework of these force fields, and we have therefore chosen to use approximate force constants obtained by interpolation or extrapolation of values refined for known structures. These hydrogen-bond–related constants are given in Table II. Values of f(CO) and f(H···O) were obtained using the r(N···O) distances of poly(glycine I) (Dwivedi and Krimm, 1982*b*) and β-poly(L-alanine) (Dwivedi and Krimm, 1982*a*) as reference points, while f(NH ob) and f(NH···O ib) were estimated by comparisons between β-poly(L-alanine) and α-poly(L-alanine) (Dwivedi and Krimm, 1984*b*).

The force field described thus far includes intrachain valence force constants and interchain hydrogen bond force constants. In an early analysis of the spectra of poly(glycine I) (Abe and Krimm, 1972) it was found that such a force field could not account for splittings in infrared amide I and amide II modes, and that transition dipole coupling had to be introduced to explain such splittings (Krimm and Abe, 1972). This theory, and its extension (Moore and Krimm, 1975), can be applied to all-L infinite-chain polypeptides (such as an α-helix or β-sheet) even without a normal mode analysis: helical symmetry uniquely defines the relative eigenvector components in each symmetry species. This is no longer the case for an alternating L,D polypeptide chain: the L,D dipeptide is the asymmetric unit, and only a normal mode calculation can determine the relative eigenvector components. A more general formulation of transition dipole coupling (Cheam and Krimm, 1984) shows how these components can be used, and we have employed this theory to determine amide I and II mode splittings of β-helices (Naik, 1984). The effective transition dipole moment for amide I was taken to be 0.45 Debye. This is slightly higher than the 0.37 D of β-poly(L-alanine) (Dwivedi and Krimm, 1982*a*), but was chosen because it gives better agreement with the observed frequencies and splittings of poly(γ-benzyl-L,D-glutamate) (Lotz et al., 1976). The effective moment for amide II was 0.269 D, the same as that used for β-poly(L-alanine). Transition moments were summed within a radius of $> \pm 30$ Å.

Calculations

Of the calculated eigenfrequencies, we have selected the amide I, II, III, and V for presentation here. These peptide group modes are particularly sensitive to the conformation of the backbone, and should provide an optimum means of characterizing structure. A more complete listing of the normal modes can be found in Naik (1984).

We have also used the eigenvectors of the amide I modes to compute the relative intensities of the A (polarized parallel to the helix axis) and E_1 (polarized perpendicular to the helix axis) species infrared modes. This provides information for calculating dichroic ratios (absorbance parallel/absorbance perpendicular), which can be compared with polarized measurements on oriented samples (Lotz et al., 1976). The transition moment associated with CO stretch (s) in a given normal mode is proportional to the CO s eigenvector component. We have taken the magnitude of this transition moment as equal to the product of the effective transition dipole moment and the corresponding CO s eigenvector component for this normal mode (from the L matrix). The orientation of the transition moment was taken to be the same as in β-(poly(L-alanine) (Moore and Krimm, 1976). The components of these vectors along and perpendicular to the helix axis were summed for the translational repeat along the axis, taking due account of the proper phases between adjacent L,D units (i.e., 0 for the A species modes and ψ for the E_1 species modes, where ψ is the rotation angle between units about the helix axis). The intensity is proportional to the square of this sum, and all of the component intensities have been normalized to the highest intensity (A species) component, $\nu^*(A)$.

TABLE II
HYDROGEN BOND FORCE CONSTANTS FOR β-HELICES*

Force Constant‡		$\beta^{4.4}$	$\beta^{5.3}$	$\beta_G^{5.3}$	$\uparrow\downarrow\beta^{5.6}$	$\uparrow\downarrow\beta^{7.2}$	$\uparrow\uparrow\beta^{5.6}$	$\uparrow\uparrow\beta^{7.2}$
f(CO)	A§	9.990	10.030	10.080	10.000	10.029	10.110	10.200
	B	10.020	10.000	10.060			9.882	10.110
f(H···O)	A	0.145	0.124	0.100	0.140	0.120	0.100	0.100
	B	0.120	0.143	0.110			0.140	0.100
f(NH···O ib)	A	0.030	0.020	0.020	0.030	0.020	0.020	0.020
	B	0.020	0.020	0.020			0.036	0.020
f(NH ob)	A	0.145	0.129	0.129	0.142	0.129	0.140	0.129
	B	0.129	0.129	0.129			0.157	0.129

*Force constants that differ from those of β-poly(L-alanine) with the CH_3 group approximated by a point mass (Dwivedi and Krimm, 1984*a*). See text for method of determination.

‡f(CO) and f(H···O) refer to CO and H···O stretch, respectively, and are given in millidynes per angstrom. ib = in-plane bend, ob = out-of-plane bend; these force constants are in millidyne × angstrom.

§A: D′ → D hydrogen bond; B: L → L′ hydrogen bond.

RESULTS

Single-stranded Helices

The $\beta^{4,4}$-helix has (in our approximation of a side-chain point mass) 14 atoms in the L,D chemical unit. There are 40 normal modes of A symmetry, 41 doubly degenerate modes of E_1 symmetry, and 42 doubly degenerate modes of E_2 symmetry. Modes of A and E_1 symmetry are active in both Raman and infrared spectra while modes of E_2 symmetry are only Raman active.

In Table III we present the calculated amide I, II, III, and V frequencies for the $\beta^{4,4}$-helix as well as the potential energy distribution (PED) for each mode. In most cases only contributions to the PED that are $\geq$10% have been included, although in some instances PEDs between the 5% and 10% level have also been given to present a more

TABLE III
CALCULATED AMIDE FREQUENCIES OF THE $\beta^{4,4}$-HELIX

Mode	Species			Potential energy distribution*
	A	E_1	E_2	
		cm^{-1}		
I			1,681	CO(L)s(68) CN(L)s(19) CO(D)s(8) $C^{\alpha}CN$(L)d(6)
			1,672	CO(D)s(68) CN(D)s(18) CO(L)s(8) $C^{\alpha}CN$(D)d(7)
		1,653		CO(L)s(67) CN(L)s(19) CO(D)s(8) $C^{\alpha}CN$(L)d(6)
	1,648			CO(L)s(68) CN(L)s(19) CO(D)s(7) $C^{\alpha}CN$(L)d(6)
		1,644		CO(D)(68) CN(D)s(18) CO(L)s(8) $C^{\alpha}CN$(D)d(6)
	1,631			CO(D)s(69) CN(D)s(18) CO(L)s(7) $C^{\alpha}CN$(D)d(6)
II		1,564		NH(L)ib(30) NH(D)ib(18) CN(L)s(12) CN(D)s(8)
			1,543	NH(D)ib(26) NH(L)ib(20) CN(D)s(13) $C^{\alpha}CN$(D)s(10) CN(L)s(8)
	1,540			NH(D)ib(25) NH(L)ib(21) CN(D)s(13) $C^{\alpha}C$(D)s(10) CN(L)s(9)
			1,538	NH(L)ib(27) NH(D)ib(20) CN(L)s(12) CN(D)s(8)
		1,538		NH(D)ib(28) NH(L)ib(18) CN(D)s(14) CN(L)s(9)
	1,534			NH(L)ib(26) NH(D)ib(21) CN(L)s(12) CN(D)s(9)
III		1,363		H^{α}(L)b2(26) NH(D)ib(16) NH(L)ib(13) $C^{\alpha}C$(D)s(12)
			1,359	H^{α}(L)b2(23) H^{α}(D)b2(17) NH(D)ib(15) $C^{\alpha}C$(D)s(10) NH(L)ib(10)
	1,358			H^{α}(L)b2(23) H^{α}(D)b2(19) NH(D)ib(14) $C^{\alpha}C$(D)s(10) NH(L)ib(10)
		1,330		H^{α}(D)b2(37) NH(L)ib(14) NH(D)ib(11)
			1,328	NH(L)ib(20) NH(D)ib(16) $C^{\alpha}C^{\beta}$(L)s(14) $C^{\alpha}C$(L)s(10)
	1,327			NH(L)ib(21) NH(D)ib(17) $C^{\alpha}C^{\beta}$(L)s(16)
		1,249		H^{α}(L)b2(50) $C^{\alpha}C^{\beta}$(L)s(12) NH(L)ib(8)
		1,224		H^{α}(D)b2(37) $C^{\alpha}C^{\beta}$(D)s(10) CN(L)s(10) NH(D)ib(8) NH(L)ib(7)
	1,218			$C^{\alpha}C^{\beta}$(D)s(22) H^{α}(L)b2(20) H^{α}(D)b2(15) NH(L)ib(13) NC^{α}(L)s(12) CN(L)s(7)
			1,218	$C^{\alpha}C^{\beta}$(D)s(22) H^{α}(L)b2(19) H^{α}(D)b2(16) NH(L)ib(13) NC^{α}(L)s(12) CN(L)s(7)
			1,187	$C^{\alpha}C^{\beta}$(L)s(36) $C^{\alpha}C^{\beta}$(D)s(12) H^{α}(D)b1(12) NC^{α}(L)s(8) CN(L)s(8) NH(D)ib(7)
	1,186			$C^{\alpha}C^{\beta}$(L)s(47) H^{α}(D)b1(16) CN(L)s(8) NC^{α}(L)s(8) NH(D)ib(8)
	1,181			$C^{\alpha}C^{\beta}$(D)s(39) CN(D)s(16) H^{α}(D)b2(12) NC^{α}(D)s(9) NH(D)ib(9)
			1,181	$C^{\alpha}C^{\beta}$(D)s(27) CN(D)s(14) $C^{\alpha}C^{\beta}$(L)s(12) NC^{α}(D)s(10) H^{α}(D)b2(10) NH(D)ib(10)
		1,179		$C^{\alpha}C^{\beta}$(L)s(33) NC^{α}(D)s(16) NH(D)ib(13) H^{α}(D)b1(11) CN(D)s(10)
V			735	CN(D)t(62) NH(D)ob(28) NH···O(D)d(16)
	734			CN(D)t(64) NH(D)ob(30) NH···O(D)d(16)
		733		NH(D)ob(22) CN(D)t(22) CO(D)ob(16)
		720		$C^{\alpha}C$(L)s(20) CO(D)ib(11) NH(D)ob(10)$NC^{\alpha}C$(D)d(10)
			685	CN(L)t(75) NH(L)ob(32) NH···O(L)d(12)
	683			CN(L)t(74) NH(L)ob(34) NH···O(L)d(12)
		680		CN(L)t(65) NH(L)ob(34) NH···O(L)d(12)

*s = stretch, d = deformation, ib = in-plane bend, ob = out-of-plane bend, t = torsion. Number in parentheses is (unnormalized) contribution of internal coordinate to potential energy change in normal mode.

complete physical picture of the mode. In the case of amide III we have presented all modes in which there is a ≥5% contribution of NH in-plane bend (ib). This should encompass the main *N*-deuteration–sensitive bands, since there is evidence of such sensitivity even at the 5–10% level (Naik and Krimm, 1984*c*). For amide V, we have given those modes over 500 cm^{-1} that have a ≥10% contribution from NH out-of-plane bend (ob), generally accompanied by a significant CN torsion (t) component. Relative intensities of parallel and perpendicular components, and dichroic ratios, of amide I modes are given in Table IV.

TABLE IV
CALCULATED INFRARED INTENSITIES, AND DICHROIC RATIOS, FOR AMIDE I MODES OF β-HELIX STRUCTURES

Structure	Species	ν	Relative intensity*		Dichroic Ratio‡
			Parallel	Perpendicular	
		cm^{-1}			
$\beta^{4.4}$	A	1,648	0.286	0.113	2.530
		1,631	1.000	0.097	10.329
	E_1	1,653	0.009	0.020	0.428
		1,644	0.002	0.054	0.030
$\beta^{6.3}$	A	1,652	0.133	0.167	0.796
		1,643	1.000	0.018	55.314
	E_1	1.654	0.000_2	0.044	0.005
		1,645	0.000_2	0.004	0.061
$\beta_G^{6.3}$	A	1,648	1.000	0.122	8.224
		1,647	0.318	0.044	7.300
	E_1	1,650	0.000_1	0.046	0.002
		1,649	0.000_3	0.000_1	2.316
$\uparrow\downarrow\beta^{5.6}$	A	1,672	0.003	0.040	0.086
		1,669	0.242	0.012	19.490
		1,666	0.362	0.004	96.110
		1,636	1.000	0.754	1.327
	E_1	1,675	0.004	0.223	0.017
		1,669	0.004	0.042	0.101
		1,666	0.004	0.041	0.100
		1,656	0.003	0.003	1.364
$\uparrow\downarrow\beta^{7.2}$	A	1,686	0.022	0.005	4.127
		1,674	0.031	0.056	0.553
		1,667	0.003	0.070	0.049
		1,632	1.000	0.174	5.733
	E_1	1,677	0.003	0.055	0.055
		1,674	0.003	0.031	0.083
		1,662	0.003	0.015	0.164
		1,651	0.004	0.051	0.059
$\uparrow\uparrow\beta^{5.6}$	A	1,705	0.002	0.172	0.010
		1,669	0.402	0.082	4.891
		1,668	0.370	0.733	0.505
		1,656	1.000	0.131	7.648
	E_1	1,697	0.001	0.016	0.033
		1,685	0.000	0.061	0.001
		1,683	0.002	0.233	0.008
		1,664	0.007	0.052	0.128
$\uparrow\uparrow\beta^{7.2}$	A	1,724	0.000	0.023	0.000
		1,686	0.020	0.011	1.860
		1,676	1.000	0.128	7.796
		1,670	0.001	0.302	0.005
	E_1	1,712	0.000_1	0.003	0.032
		1,698	0.000	0.009	0.000
		1,682	0.000	0.095	0.000
		1,669	0.003	0.036	0.084

*Normalized to largest A species intensity; rounded to third decimal.
‡I(∥)/I(⊥), based on non-rounded values.

TABLE V
CALCULATED AMIDE FREQUENCIES OF THE $\beta^{6.3}$-HELIX

Mode	Species		
	A	E_1	E_2
	cm^{-1}	cm^{-1}	cm^{-1}
I	1,652(10 63)*	1,654(— 69)	1,652(— 70)
	1,643(63 10)	1,645(69 —)	1,652(70 —)
II	1,570(30 12)	1,572(32 13)	1,573(32 13)
	1,542(16 35)	1,559(14 33)	1,557(14 33)
III	1,376(8 7)	1,442(— 7)	1,439(— 8)
	1,321(16 12)	1,401(8 5)	1,406(8 —)
	1,264(14 17)	1,303(19 —)	1,301(20 —)
	1,201(5 —)	1,266(11 22)	1,266(10 23)
	1,182(— 6)	1,207(5 —)	1,208(5 —)
		1,187(— 7)	1,187(— 7)
V	698(— 24)	698(— 22)	696(— 24)
	677(35 —)	677(24 —)	678(17 —)
	574(— 12)	658(13 —)	644(21 —)

*The numbers in parentheses give a condensed form of the PED: the CO stretch contribution for amide I, the NH in-plane bend contribution for amide II and amide III, and the NH out-of-plane bend contribution for amide V. The two numbers refer to the contributions from the L and D peptide groups, respectively.

The number of atoms per L,D chemical unit of the $\beta^{6.3}$-helix is the same as for the $\beta^{4.4}$-helix, and therefore the number of computed frequencies in each symmetry species is also the same. The calculated amide I, II, III, and V frequencies (and condensed PEDs) for the $\beta^{6.3}$-helix are given in Table V, and relative intensities and dichroic ratios for amide I modes are given in Table IV. As mentioned above, to determine the effects of conforma-

TABLE VI
CALCULATED AMIDE FREQUENCIES OF THE $\beta_G^{6.3}$-HELIX

Mode	Species		
	A	E_1	E_2
	cm^{-1}	cm^{-1}	cm^{-1}
I	1,648(8 69)*	1,650(— 74)	1,659(74 —)
	1,647(68 8)	1,649(73 —)	1,650(— 74)
II	1,560(14 35)	1,559(13 36)	1,557(13 36)
	1,557(36 13)	1,555(37 12)	1,556(38 12)
III	1,380(8 11)	1,370(8 12)	1,367(8 13)
	1,309(21 19)	1,337(13 11)	1,342(13 10)
	1,229(9 10)	1,260(11 —)	1,256(13 —)
		1,232(6 14)	1,223(— 16)
V	587(47 —)	592(26 9)	590(35 7)
	557(— 31)	585(23 22)	584(15 27)
		544(— 10)	

*The numbers in parentheses give a condensed form of the PED: the CO stretch contribution for amide I, the NH in-plane bend contribution for amide II and amide III, and the NH out-of-plane bend contribution for amide V. The two numbers refer to the contributions from the L and D peptide groups, respectively.

TABLE VII
CALCULATED AMIDE FREQUENCIES OF THE $\uparrow\downarrow\beta^{5,6}$-HELIX

Mode	Species			Potential energy distribution*
	A	E_1	E_2	
		cm^{-1}		
I		1,675		CO(D')s(38) CO(D)s(32) CN(D')s(11) CN(D)s(9)
			1,674	CO(L')s(70) CN(L')s(19) $C^{\alpha}CN$(L')d(7) CO(D')s(5)
			1,674	CO(D')s(68) CN(D')s(20) CO(L')s(6) $C^{\alpha}CN$(D')d(6)
	1,672			CO(D)s(53) CO(D')s(22) CN(D)s(16) CN(D')s(7)
			1,671	CO(L)s(76) CN(L)s(20) $C^{\alpha}CN$(L)d(7)
	1,669			CO(L')s(67) CN(L')s(19) CO(D')s(7) $C^{\alpha}CN$(L')d(6)
		1,669		CO(L')s(71) CN(L')s(19) $C^{\alpha}CN$(L')d(7)
	1,666			CO(L)s(72) CN(L)s(20) $C^{\alpha}CN$(L)d(7)
		1,666		CO(L)s(74) CN(L)s(20) $C^{\alpha}CN$(L)d(7)
			1,662	CO(D)s(72) CN(D)s(21) $C^{\alpha}CN$(D)d(7)
		1,656		CO(D)s(43) CO(D')s(31) CN(D)s(13) CN(D')s(9)
	1,636			CO(D')s(43) CO(D)s(20) CN(D')s(12) CO(L')s(9) CN(D)s(6) CO(L)s(5)
II		1,553		NH(L)ib(31) NH(D)ib(16) CN(L)s(11) CN(D)s(6)
		1,550		NH(D')ib(26) NH(L')ib(20) CN(D')s(10) CN(L')s(6)
	1,547			NH(D')ib(39) CN(D')s(15) $C^{\alpha}C$(D')s(12) CO(D')ib(9) NH(L)ib(5)
			1,547	NH(D')ib(29) NH(L')ib(20) CN(D')s(11) CN(L')s(6)
	1,547			NH(L)ib(36) CN(L)s(14) $C^{\alpha}C$(L)s(9) NH(D)ib(7) CO(L)ib(7) NH(D')ib(5)
			1,546	NH(L)ib(33) NH(D)ib(16) CN(L)s(12) CN(D)s(6)
			1,544	NH(L')ib(30) NH(D')ib(18) CN(L')s(14) CN(D')s(7)
			1,543	NH(D)ib(31) NH(L)ib(17) CN(D)s(12) CN(L)s(8)
		1,542		NH(L')ib(27) NH(D')ib(18) CN(L')s(13) CN(D')s(7)
		1,541		NH(D)ib(29) NH(L)ib(15) CN(D)s(11) CN(L)s(8)
	1,535			NH(L')ib(37) CN(L')s(15) NH(L)ib(9)
	1,531			NH(D)ib(32) CN(D)s(12) NH(L')ib(10) $C^{\alpha}C$(D)s(7) NH(L)ib(7)
III	1,386			H^{α}(D')b2(13) H^{α}(L')b2(13) H^{α}(L)b2(11) H^{α}(D)b2(10) $C^{\alpha}C$(D')s(6) NH(D')ib(6)
	1,385			H^{α}(L)b2(14) H^{α}(D)b2(13) H^{α}(L')b2(11) H^{α}(D')b2(10) NH(D)ib(6)
			1,378	H^{α}(D')b2(17) H^{α}(L')b2(11) H^{α}(D)b2(9) NH(D')ib(8) $C^{\alpha}C$(D')s(7) H^{α}(L)b2(6) $C^{\alpha}C$(L')s(5) NH(L')ib(5)
			1,377	H^{α}(D)b2(17) H^{α}(L)b2(12) H^{α}(D')b2(9) NH(D)ib(8) $C^{\alpha}C$(D)s(6) H^{α}(L')b2(6) $C^{\alpha}C$(L)s(5) NH(L)ib(5)
		1,374		H^{α}(D')b2(17) H^{α}(D)b2(12) H^{α}(L')b2(8) NH(D')ib(8) NH(D)ib(6) H^{α}(L)b2(5)
		1,373		H^{α}(D)b2(17) H^{α}(D')b2(12) NH(D)ib(9) H^{α}(L)b2(8) $C^{\alpha}C$(D)s(6) NH(D')ib(6) H^{α}(L')b2(5)
		1,341		H^{α}(L')b2(23) H^{α}(L)b2(13) NH(L')ib(9) H^{α}(D')b2(6) NH(D')ib(5)
		1,340		H^{α}(L)b2(24) H^{α}(L')b2(13) NH(L)ib(9) H^{α}(D)b2(6)
			1,334	H^{α}(L')b2(25) H^{α}(D')b2(11) NH(L')ib(11)
			1,333	H^{α}(L)b2(26) NH(L)ib(11) H^{α}(D)b2(10) NH(D)ib(8)
	1,312			H^{α}(D')b2(21) H^{α}(L')b2(19) NH(L')ib(14) NH(D')ib(12)
	1,309			H^{α}(D)b2(21) H^{α}(L)b2(19) NH(L)ib(14) NH(D)ib(13)
	1,288			H^{α}(D)b2(15) H^{α}(L)b2(13) CO(D)ib(8) CN(D)s(7) H^{α}(L)b1(6) NH(L)ib(6) CO(L)ib(5) NH(D)ib(5)
	1,284			H^{α}(D')b2(16) H^{α}(L')b2(12) CN(D')s(8) CO(D')ib(8) H^{α}(L')b1(6) NH(D')ib(6) NH(L')ib(6)
			1,271	H^{α}(D)b2(32) NH(L)ib(12)
			1,268	H^{α}(D')b2(32) NH(L')ib(10)
		1,267		H^{α}(D)b2(36) NH(L)ib(12)
		1,265		H^{α}(D')b2(37) NH(L')ib(11)
	1,240			$C^{\alpha}C^{\beta}$(D)s(15) H^{α}(D)b2(15) H^{α}(L)b2(15) NH(D)ib(10)
			1,238	H^{α}(L)b2(21) NH(D)ib(16) $C^{\alpha}C^{\beta}$(D)s(10)
		1,237		H^{α}(L)b2(23) NH(D)ib(18)
		1,236		H^{α}(L')b2(23) NH(D')ib(16)

TABLE VII (Continued)

Mode	Species			Potential energy distribution*
	A	E_1	E_2	
			1,236	H^{α}(L')b2(22) NH(D')ib(14) $C^{\alpha}C^{\beta}$(D')s(9) H^{α}(D')b2(7) CN(L')s(7) NC^{α}(D')s(6) NH(L')ib(6)
V	725			CO(D)ob(16) CN(L')t(13) NH(L')ob(10) CO(D')ob(9) NH(L)ob(6) CN(L)t(5)
		720		CN(L')t(38) CN(L)t(31) NH(L')ob(19) NH(L)ob(15)
			719	CN(L')t(39) CN(L)t(30) NH(L')ob (18) NH(L)ob(14)
	717			CN(L')t(33) CN(L)t(18) NH(L')ob(16) NH(L)ob(7)
		717		CN(L)t(23) CN(L')t(19) NH(L)ob(13) NH(L')ob(11)
			716	CN(L)t(24) NH(L)ob(16) CN(L')t(16) NH(L')ob(13)
	714			CN(L)t(30) NH(L)ob(21) CN(L')t(12) NH(L')ob(11)
	712			CN(D')t(42) NH(D')ob(26) CO(L')ob(10) NH· · ·O(D')d(10)
			708	CN(D')t(23) NH(D')ob(15)
		707		CN(D')t(20) NH(D')ob(14)
		695		CN(D)t(25) CO(D)ib(18) $C^{\alpha}C$(D)s(15) NH(D)ob(13) $NC^{\alpha}C$(D)d(11)
			694	CN(D)t(36) ND(D)ob(17) CO(D)ib(15) $C^{\alpha}C$(D)s(12)
	692			CN(D)ob(55) NH(D)ob(28) NH· · ·O(D)d(13)
		656		CO(L')ob(24) CN(D)t(13) NH(D)ob(10)
		640		CN(D')t(18) $C^{\alpha}C$(L)s(15) CO(L)ib(13) CO(L')ob(13) NH(D')ob(10)
			637	$C^{\alpha}C$(L)s(17) CO(L)ib(16) CN(D')t(14) NH(D')ob(8) CN(D)t(8) CO(L')ob(6) NH(D)ob(6)

*s = stretch, d = deformation, ib = in-plane bend, ob = out-of-plane bend, t = torsion. Number in parenthesis is (unnormalized) contribution of internal coordinate to potential energy change in normal mode. L and D refer to residues on one chain, L' and D' to residues on the second chain.

tional changes that result in a helix of the same symmetry, we have also calculated the normal modes of the goniometric $\beta_G^{6,3}$-helix (Colonna-Cesari et al., 1977). Its amide mode frequencies (and condensed PEDs) are given in Table VI, and amide I intensities and dichroic ratios are given in Table IV.

Double-stranded Helices

In the double-stranded helices there are 28 atoms in the L,D units of the chains, and this leads to 82 Raman and infrared active modes of A symmetry, 83 Raman and infrared active doubly degenerate modes of E_1 symmetry, and 84 Raman active doubly degenerate modes of E_2 symmetry. The amide I, II, III, and V mode frequencies (with full PEDs) of $\uparrow\downarrow\beta^{5,6}$ are given in Table VII and amide I intensities and dichroic ratios are given in Table IV. The amide mode frequencies (and condensed PEDs) of $\uparrow\downarrow\beta^{7,2}$ are given in Table VIII and amide I intensities and dichroic ratios are given in Table IV. For the comparable parallel double-stranded structures, the amide mode frequencies (and condensed PEDs) are given in Tables IX and X for $\uparrow\uparrow\beta^{5,6}$ and $\uparrow\uparrow\beta^{7,2}$, respectively, and amide I intensities and dichroic ratios for both are given in Table IV.

DISCUSSION

Single-stranded Helices

The amide I modes are essentially CO s, and since the CO groups are nearly parallel to the helix axis, the most intense infrared bands are expected to be A-species modes. These, as well as other species modes of the single-stranded helices, show a significant dependence of frequency on structure, due in part to the different geometries but mainly to the differing effects of transition dipole coupling (Krimm and Abe, 1972). Thus, the frequencies calculated for $\beta^{4,4}$ before including such coupling are 1,681 and 1,679 cm^{-1}, the same for A, E_1, and E_2 species, while after including the coupling a spread of 50 cm^{-1} is obtained, the frequency shift (which is negative because of the energetically favorable, namely, parallel, alignment of amide I transition dipoles) now being species-dependent. The predicted intensity pattern (see Table IV) is such that a splitting of 1,648(A)–1,631(A) = 17 cm^{-1} might be expected to be seen; if polarized radiation were used on an oriented sample, both parallel and perpendicular components at 1,648 cm^{-1} should be observable. Incidentally, it is important to note that each of the unperturbed frequencies is associated with an amide I mode localized mainly on an L or D residue. This is quite different from the situation for a linearly extended polypeptide chain of all L (or all D) residues, where symmetry requires both peptide groups in the structural repeat unit to have equal amide I eigenvector components. It is therefore not possible to use the latter system as a model for helical L,D polypeptides, as has been done (Sychev et al., 1980); correct eigenvectors can only be obtained from a full normal mode calculation.

The amide I modes of the $\beta^{6,3}$-helix demonstrate a similar effect. Here the unperturbed frequencies are 1,688

TABLE VIII
CALCULATED AMIDE FREQUENCIES OF THE $\uparrow\downarrow^{7,2}$-HELIX

Mode	Species		
	A	E_1	E_2
	cm^{-1}	cm^{-1}	cm^{-1}
I	1,686 (28 20 13 16)*	1,677 (18 12 22 25)	1,675 (— 14 16 44)
	1,674 (— — 38 31)	1,674 (— — 38 28)	1,674 (53 18 — —)
	1,667 (28 42 — —)	1,662 (23 43 — 5)	1,671 (22 36 7 11)
	1,632 (19 10 22 27)	1,651 (33 16 11 17)	1,667 (— 8 50 17)
II	1,556 (45 — — —)	1,556 (13 — 30 6)	1,559 (8 — 35 8)
	1,554 (— — 41 8)	1,555 (33 — 12 —)	1,555 (39 — 7 —)
	1,537 (— — 9 42)	1,552 (— — 10 40)	1,549 (— — 10 40)
	1,537 (6 45 — —)	1,549 (5 44 — —)	1,547 (— 44 — —)
III	1,316 (— — 11 11)	1,393 (— 5 — —)	1,379 (— — — 9)
	1,314 (9 10 — —)	1,392 (— — — 5)	1,378 (— 10 — —)
	1,296 (12 11 — —)	1,344 (— — 7 7)	1,365 (9 6 — —)
	1,294 (— — 9 10)	1,344 (7 7 — —)	1,364 (— — 8 7)
	1,246 (7 11 — —)	1,274 (15 7 — —)	1,266 (17 — — —)
	1,244 (— — 7 10)	1,273 (— — 13 7)	1,265 (— — 15 —)
		1,245 (— 16 — —)	1,245 (— 22 — —)
		1,244 (— — — 15)	1,244 (— — — 20)
V	680 (— — — 16)	684 (— — — 13)	637 (— 20 — —)
	668 (6 5 — —)	643 (— 13 — 9)	631 (23 — 11 —)
	658 (— 14 — —)	634 (— 8 16 —)	626 (10 6 23 —)
	629 (— 7 6 —)	627 (29 — — —)	618 (— — — 13)
	625 (23 — — —)	617 (— 8 13 7)	
	616 (— 8 20 —)		

*The numbers in parentheses give a condensed form of the PED: the CO stretch contribution for amide I, the NH in-plane bend contribution for amide II and amide III, and the NH out-of-plane bend contribution for amide V. The four numbers refer to the contributions from the L, D, L′ and D′ peptide groups, respectively.

TABLE IX
CALCULATED AMIDE FREQUENCIES OF THE $\uparrow\uparrow\beta^{5,6}$-HELIX

Mode	Species		
	A	E_1	E_2
	cm^{-1}	cm^{-1}	cm^{-1}
I	1,705 (— 33 — 43)*	1,697 (57 — 18 —)	1,690 (— 7 — 69)
	1,669 (72 — — —)	1,685 (— 25 — 51)	1,685 (21 — 54 —)
	1,668 (— 43 — 33)	1,683 (— 51 — 25)	1,684 (— 69 — 7)
	1,656 (— — 72 —)	1,664 (18 — 54 —)	1,680 (54 — 21 —)
II	1,546 (— 19 — 30)	1,560 (— 33 — 15)	1,555 (— 41 — 7)
	1,546 (28 — 23 —)	1,555 (— 15 — 34)	1,553 (— 7 — 42)
	1,545 (— 30 — 19)	1,544 (27 — 23 —)	1,544 (19 — 31 —)
	1,540 (23 — 28 —)	1,542 (24 — 27 —)	1,542 (31 — 19 —)
III	1,379 (5 9 — —)	1,369 (— 14 — —)	1,372 (5 14 — —)
	1,378 (— — 5 9)	1,368 (— — — 13)	1,371 (— — 6 13)
	1,317 (12 10 7 6)	1,343 (10 — 5 —)	1,336 (12 8 — —)
	1,315 (6 5 12 10)	1,342 (6 — 9 —)	1,336 (— — 12 8)
	1,234 (— — 8 7)	1,263 (— — 10 6)	1,267 (— — 8 7)
	1,233 (8 7 — —)	1,261 (10 6 — —)	1,266 (8 7 — —)
		1,238 (— — 7 12)	1,236 (— — 7 11)
		1,237 (7 11 — —)	1,235 (8 10 — —)
V	763 (15 — 11 —)	771 (13 — 11 —)	775 (9 — 8 —)
	759 (13 — 17 —)	765 (12 — 14 —)	765 (11 — 13 —)
	609 (— — — 11)	637 (5 — — 10)	749 (6 — 6 —)
	583 (— 15 — —)	608 (— 21 — 13)	635 (6 — — 8)
	571 (— 15 — —)	596 (— 11 — 15)	608 (— 14 — 16)
	558 (— — — 20)		594 (— 15 — 9)

*The numbers in parentheses give a condensed form of the PED: the CO stretch contribution for amide I, the NH in-plane bend contribution for amide II and amide III, and the NH out-of-plane bend contribution for amide V. The four numbers refer to the contributions from the L, D, L′, and D′ peptide groups, respectively.

TABLE X
CALCULATED AMIDE FREQUENCIES OF THE ↑↑$\beta^{7.2}$-HELIX

Mode	Species		
	A	E_1	E_2
	cm^{-1}	cm^{-1}	cm^{-1}
I	1,724 (13 28 11 25)*	1,712 (39 14 18 7)	1,695 (43 14 17 6)
	1,686 (35 15 19 9)	1,698 (14 35 8 21)	1,690 (15 7 39 17)
	1,676 (18 11 32 18)	1,682 (9 20 17 31)	1,686 (13 35 8 21)
	1,670 (12 23 16 25)	1,669 (17 9 35 18)	1,684 (7 22 14 34)
II	1,553 (26 — 26 —)	1,560 (— 26 — 24)	1,558 (— 26 — 24)
	1,546 (— 24 — 26)	1,552 (26 — 26 —)	1,557 (— 24 — 26)
	1,545 (— 25 — 24)	1,551 (— 24 — 26)	1,550 (26 — 26 —)
	1,544 (26 — 26 —)	1,550 (26 — 26 —)	1,549 (26 — 26 —)
III	1,386 (— 6 — —)	1,378 (— 6 — —)	1,366 (6 8 — —)
	1,385 (— — — 6)	1,376 (— — — 6)	1,365 (— — 6 8)
	1,310 (9 10 7 8)	1,334 (6 7 — 5)	1,351 (5 6 — —)
	1,308 (7 7 8 9)	1,332 (— 5 6 7)	1,350 (— — 5 5)
	1,238 (— — 8 9)	1,264 (— — 6 —)	1,254 (— — 13 —)
	1,238 (8 9 — —)	1,263 (6 — — —)	1,253 (13 — — —)
		1,241 (— — 5 11)	1,243 (— — — 17)
		1,240 (6 11 — —)	1,243 (— 17 — —)
V	657 (9 — 8 —)	659 (8 — 7 —)	663 (— — 7 —)
	639 (9 — 15 —)	648 (6 — 10 —)	655 (9 — — —)
	630 (8 — — —)	622 (18 — — 6)	622 (14 7 6 7)
	627 (7 — — —)	616 (— 11 10 5)	615 (— 18 9 7)
	608 (— — — 8)	608 (— 5 12 6)	608 (11 — 14 —)
	590 (— 20 — —)	598 (9 5 — 8)	598 (8 — — 15)
	574 (10 — — —)		
	564 (— — — 15)		

*The numbers in parentheses give a condensed form of the PED: the CO stretch contribution for amide I, the NH in-plane bend contribution for amide II and amide III, and the NH out-of-plane bend contribution for amide V. The four numbers refer to the contributions from the L, D, L′, and D′ peptide groups, respectively.

and 1,684 cm^{-1} (for all symmetry species), and the different structure (which also yields a slightly different set of eigenvectors) results in different shifts when coupling is introduced. The most important result, aside from the smaller spread in frequencies, namely, 9 cm^{-1}, is that the most intense band expected in the infrared spectrum, namely, the lowest frequency A species mode (cf. Table IV), is predicted at a significantly higher frequency in the $\beta^{6.3}$-helix (1,643 cm^{-1}) than in the $\beta^{4.4}$-helix (1,631 cm^{-1}). It is interesting that the amide I modes of the $\beta_G^{6.3}$-helix, whose unperturbed frequencies are 1,686 and 1,683 cm^{-1}, are predicted to be different from those of the $\beta^{6.3}$-helix. The strong infrared A species mode is slightly higher (1,648 cm^{-1}), and the potentially observable splitting between modes is significantly less: for $\beta_G^{6.3}$ it is expected to be $1{,}647(A) - 1{,}648(A) = -1$ cm^{-1}, whereas for $\beta^{6.3}$ it could be $1{,}652(A) - 1{,}643(A) = 9$ cm^{-1}.

The intensities of Raman bands are more difficult to predict at this point than those of infrared bands. However, experimental results may be of help here. Analysis of the Raman spectra of native and ion-bound crystalline GA (Naik and Krimm, 1984*b*, 1986) indicates that the strong Raman band for expected double-stranded structures is observed near the midpoint of the range of predicted frequencies remaining after exclusion of $\nu^*(A)$. If this is also true of the single-stranded helices, we would predict strong Raman bands near 1,663 cm^{-1} for $\beta^{4.4}$, near 1,650 cm^{-1} for $\beta^{6.3}$, and near 1,654 cm^{-1} for $\beta_G^{6.3}$. (This noncoincidence of strong infrared and Raman frequencies is also observed (and predicted) for parallel-chain (J. Bandekar and S. Krimm, manuscript submitted for publication) and antiparallel-chain (Dwivedi and Krimm, 1982*a*) β-sheet structures, and it is therefore not surprising that it is seen for β-helix structures.)

The amide II (essentially NH ib plus CN s) modes are strong in the infrared spectra, and weak or absent in the Raman spectra, of polypeptides. Because the transition moment of amide II is essentially perpendicular to that of amide I, the strongest infrared band will be of E_1 symmetry. As can be seen from Tables III, V, and VI, significantly different frequencies are predicted for these modes as a function of the structure, namely 1,564 and 1,538 cm^{-1} for $\beta^{4.4}$ and 1,572 and 1,559 cm^{-1} for $\beta^{6.3}$. The distinction between $\beta^{6.3}$ and $\beta_G^{6.3}$ is somewhat smaller.

The amide III mode is generally considered to involve NH ib and CN s, and to occur in the 1,300–1,200 cm^{-1} region. However, our experience (Naik et al., 1984*c*; and earlier papers in this series) indicates that an NH ib contribution, and therefore a sensitivity to N-deuteration, is characteristic of many bands in the broad range of

1,450–1,150 cm^{-1} even in the absence of a CN s component. For the single-stranded helices there is a definite dependence of this range on structure. Thus, for $\beta^{4.4}$ NH ib contributes between 1,363 and 1,179 cm^{-1}, for $\beta^{6.3}$ between 1,442 and 1,182 cm^{-1}, and for $\beta_G^{6.3}$ between 1,380 and 1,229 cm^{-1}. Furthermore, if the intensity decrease of a band on *N*-deuteration is related to the magnitude of the total NH ib contribution to the mode, then specific frequency regions are expected to be affected differently for the different structures. Thus, the largest NH ib contributions are expected to occur near 1,360 and 1,328 cm^{-1} for $\beta^{4.4}$, near 1,320, 1,302, and 1,265 cm^{-1} for $\beta^{6.3}$, and near 1,380, 1,369, 1,340, 1,309, and 1,231 cm^{-1} for $\beta_G^{6.3}$. Since there is a large degree of nonoverlap in the values and patterns of these frequencies, it is reasonable to expect that *N*-deuteration sensitivity in this region may provide another determinant of structure from the vibrational spectrum.

The patterns of amide V (CN t plus NH ob) modes, and therefore the sensitivity to *N*-deuteration, are also different for the different structures. The regions expected to be significantly affected by *N*-deuteration are near 734 and 683 cm^{-1} for $\beta^{4.4}$, near 697, 677, and 664 cm^{-1} for $\beta^{6.3}$, and near 591, 585, and 557 cm^{-1} for $\beta_G^{6.3}$. Again, these frequencies are sufficiently different so that there is a reasonable expectation of using the amide V region to distinguish between the single-stranded structures. This is somewhat hampered, as is the case for the amide II modes, by the present difficulty in assessing the relative intensities of these complex modes (the success in reproducing intensities for poly(glycine I) (Cheam and Krimm, 1985), however, gives hope that this can be done in the future). Nevertheless, when the patterns of amide I, II, III, and V modes are considered together, a strong case can be made for the possibility of assigning structure from the vibrational spectra of these single-stranded helices.

Double-stranded Helices

Antiparallel-Chain Structures. Since there are two chains in the asymmetric unit of double-stranded helices, there are twice as many amide modes as in the single-stranded structures. The amide I modes involve cooperative CO stretches on the L and D peptide groups of the two chains, but, as can be seen from Tables VII and VIII, the eigenvector components are far from being equal, in distinction to the situation for the antiparallel-chain pleated sheet (Dwivedi and Krimm, 1982*b*). The assumption of such equality (Sychev et al., 1980) leads to incorrect transition dipole interactions, and in fact to larger amide I frequency splittings than we find. Our calculations predict $\nu^*(A)$ at a slightly higher frequency for the $\uparrow\downarrow\beta^{5.6}$-helix (1,636 cm^{-1}) than for the $\uparrow\downarrow\beta^{7.2}$ (1,632 cm^{-1}) (these frequencies being 1,664 and 1,667 cm^{-1}, respectively, before transition dipole coupling is incorporated). The splitting between $\nu^*(A)$ and other high intensity modes is smaller for $\uparrow\downarrow\beta^{5.6}$, 30–33 up to 39 cm^{-1}, than for $\uparrow\downarrow\beta^{7.2}$, 42–45 up to (weakly) 54 cm^{-1} (with the predicted splittings before transition dipole coupling being 0 and 1 cm^{-1}, respectively). The Sychev et al. (1980) calculations give 64 cm^{-1} for the comparable splittings in both structures. It is worth noting that the observed maximum splitting might be less evident in the unpolarized spectrum of $\uparrow\downarrow\beta^{5.6}$ because of the contributions of the intervening strong bands at 1,669(A) and 1,666(A) cm^{-1} (see Table IV). In any case, these splittings are much larger than those expected for the single-stranded structures.

As noted above, intense amide I Raman bands are observed near the midpoint of the range of predicted frequencies remaining after exclusion of $\nu^*(A)$. For $\uparrow\downarrow\beta^{5.6}$ this would be 1,666 cm^{-1}, and for $\uparrow\downarrow\beta^{7.2}$ it would be 1,669 cm^{-1}.

If, as discussed for the single-stranded helices, the strongest amide II modes are expected to be infrared active modes of E_1 symmetry, then slightly different frequency ranges are predicted for the two structures. For the $\uparrow\downarrow\beta^{5.6}$-helix the E_1 species amide II modes occur in the range of 1,553–1,541 cm^{-1}, while for the $\uparrow\downarrow\beta^{7.2}$ helix this range is 1,556–1,549 cm^{-1}.

Contributions of NH ib occur in essentially the same amide III frequency regions in both the $\uparrow\downarrow\beta^{5.6}$- and $\uparrow\downarrow\beta^{7.2}$-helix structures, namely, ~1,390–1,240 cm^{-1}, but they are distributed somewhat differently. For $\uparrow\downarrow\beta^{5.6}$, large contributions are predicted for modes near 1,310 and 1,236 cm^{-1}, whereas for $\uparrow\downarrow\beta^{7.2}$ such contributions are more broadly distributed, namely, near 1,315, 1,295, 1,274, 1,266, and 1,245 cm^{-1}.

As in the case of the single-stranded helices, the amide V modes expected to be sensitive to *N*-deuteration are predicted at significantly different frequencies for the two structures. For the $\uparrow\downarrow\beta^{5.6}$-helix, modes with large NH ob contributions are calculated near 720–712 and 692 cm^{-1}, whereas for the $\uparrow\downarrow\beta^{7.2}$-helix such modes are predicted near 643, 634, 626, and 617 cm^{-1}. Such different patterns of sensitivity to *N*-deuteration should be detectable, assuming, of course, the absence of interference from other modes.

Parallel Chain Structures. The unperturbed amide I modes of $\uparrow\uparrow\beta^{5.6}$ are calculated at 1,686(A, E_1) and 1,667(A,E_1) cm^{-1}; transition dipole coupling spreads these over the range of 1,705–1,656 cm^{-1}. For $\uparrow\uparrow\beta^{7.2}$, the unperturbed amide I modes are at 1,694(A), 1,693(E_1), 1,691(A, E_1), and 1,690(A, E_1) cm^{-1}, which are spread over the range of 1,724–1,669 cm^{-1} by transition dipole coupling. The $\nu^*(A)$ mode is calculated at 1,656 cm^{-1} for the $\uparrow\uparrow\beta^{5.6}$-helix and at 1,676 cm^{-1} for the $\uparrow\uparrow\beta^{7.2}$-helix. The predicted splittings are qualitatively and quantitatively different for the two structures. For the $\uparrow\uparrow\beta^{5.6}$-helix, the largest (potentially observable) splitting is between the perpendicular component of the 1,705(A) and the parallel component of the 1,656(A) cm^{-1} bands, namely, 49 cm^{-1}, although in polarized spectra there should also be observ-

able splittings of 1,683(E_1, $\perp$) − 1,656(A, $\|$) = 27 cm^{-1}, and perhaps 1,669 (A, $\perp$) − 1,656 (A, $\|$) 13 cm^{-1}. For the $\uparrow\uparrow\beta^{7.2}$-helix, on the other hand, the strongest perpendicular component is at the lowest frequency, leading to a splitting of 1,670(A, $\perp$) − 1,676(A, $\|$) = ‡6 cm^{-1} (a weaker 1,682(E_1, $\perp$) band gives a splitting of +6 cm^{-1}). Thus, among the double-stranded helices, the parallel-chain structures have specific distinguishing characteristics: their strong A species modes are at higher frequencies, 1,656 ($\uparrow\uparrow\beta^{5.6}$) and 1,676 ($\uparrow\uparrow\beta^{7.2}$) as compared to 1,636 ($\uparrow\downarrow\beta^{5.6}$) and 1,632 ($\uparrow\downarrow\beta^{7.2}$) cm^{-1}; and their largest $\nu - \nu^*(A)$ band splittings are significantly different, 49 ($\uparrow\uparrow\beta^{5.6}$) and −6 ($\uparrow\uparrow\beta^{7.2}$) as compared to 39 ($\uparrow\downarrow\beta^{5.6}$) and 54 ($\uparrow\downarrow\beta^{7.2}$) cm^{-1}. Raman bands, on the basis of our previous analysis, would be expected at 1,685 cm^{-1} for $\uparrow\uparrow\beta^{5.6}$ and at 1,697 cm^{-1} for $\uparrow\uparrow\beta^{7.2}$, significantly different from the frequencies for the other structures.

The E_1 species amide II modes, expected to be intense in the infrared, cover a slightly larger range for $\uparrow\uparrow\beta^{5.6}$ (1,560–1,542 cm^{-1}) than for $\uparrow\uparrow\beta^{7.2}$ (1,560–1,550 cm^{-1}). Until relative intensities are determined for these modes, it will be difficult to use them for predictive purposes.

The amide III mode frequencies extend over about the same range for $\uparrow\uparrow\beta^{5.6}$ and $\uparrow\uparrow\beta^{7.2}$, being roughly comparable with the ranges for the antiparallel-chain structures. There is, however, a significant difference in the distribution of modes having large NH ib contributions: for $\uparrow\uparrow\beta^{5.6}$ these occur near 1,372, 1,336, 1,316, 1,262, and 1,236 cm^{-1}, whereas for $\uparrow\uparrow\beta^{7.2}$ these are predicted near 1,333, 1,309, and 1,240 cm^{-1}. The differences between these patterns, as well as the differences as compared to the antiparallel-chain structures, should help to identify these conformations.

The ranges and patterns of amide V modes are quite different for the two parallel-chain structures: for $\uparrow\uparrow\beta^{5.6}$ we expect large contributions of NH ob to modes near 771, 764, 608, and 595 cm^{-1}, whereas for $\uparrow\uparrow\beta^{7.2}$, such contributions are predicted near 639, 622, 616, 608, and 598 cm^{-1}.

Comparison of Predictions

To assess the spectral implications of the different β-helices discussed here, we collect in Table XI some salient results of the normal mode calculations. While these give the main features of the previous discussion, it will be important to refer to the detailed results in doing analyses of spectra.

CONCLUSIONS

It is clear, as has been noted before (Krimm, 1983), that normal mode calculations using highly predictive force fields permit fine distinctions to be made between different polypeptide chain conformations. This is supported by the present calculations on model structures for GA.

We have calculated the normal mode frequencies of three single-stranded and four double-stranded helical structures of GA that have molecular dimensions consis-

TABLE XI
COMPARISON OF AMIDE MODE PREDICTIONS FOR β-HELICES

		$\beta^{4.4}$	$\beta^{6.3}$	$\beta_G^{6.3}$	$\uparrow\downarrow\beta^{5.6}$	$\uparrow\downarrow\beta^{7.2}$	$\uparrow\uparrow\beta^{5.6}$	$\uparrow\uparrow\beta^{7.2}$
I:	$\nu^*(A)$*	1,631	1,643	1,648	1,636	1,632	1,656	1,676
	$\nu - \nu^*(A)$‡	17	9	−1	30–33, 39	42–54	13, 27, 49	−6, 6
	ν_R§	1,663	1,650	1,654	1,666	1,669	1,685	1,697
II:	$\nu(E_1)$‖	1,564	1,572	1,559	1,553–	1,556–	1,560–	1,560–
		1,538	1,559	1,555	1,541	1,549	1,542	1,550
III:	$\Delta\nu$¶	1,363–1,179	1,442–1,182	1,380–1,229	1,386–1,236	1,393–1,244	1,379–1,233	1,386–1,238
	ν(NH >15)**	1,360 (26)	1,320 (28)	1,380 (19)	1,310 (26)	1,315 (20)	1,372 (19)	1,333 (18)
		1,328 (33)	1,302 (19)	1,369 (20)	1,236 (18)	1,295 (21)	1,336 (20)	1,309 (33)
			1,265 (32)	1,340 (24)		1,274 (21)	1,316 (34)	1,240 (17)
				1,309 (40)		1,266 (16)	1,262 (16)	
				1,231 (18)		1,245 (19)	1,236 (18)	
V:	$\Delta\nu$‡‡	735–680	698–574	592–544	725–637	684–616	775–558	663–564
	ν(NH ≥20)‖‖	734 (27)	697 (23)	591 (39)	720-12 (29)	643 (22)	771 (24)	639 (24)
		683 (33)	677 (25)	585 (45)	692 (28)	634 (22)	764 (25)	622 (29)
			664 (21)	557 (31)		626 (30)	759 (30)	616 (30)
						617 (28)	608 (32)	608 (24)
							595 (25)	598 (23)

*Highest intensity infrared A species mode, in cm^{-1}.
‡Splitting between $\nu^*(A)$ and other high intensity infrared component(s).
§Expected strong Raman mode (see text).
‖Frequencies (or ranges) of E_1 species amide II modes.
¶Range of frequencies having NH ib contributions to PED ≥5%.
**Frequencies (or regions) where NH ib contribution to PED is >15%.
‡‡Range of frequencies having NH ob contributions to PED ≥5%.
‖‖Frequencies (or regions) where NH ob contribution to PED is ≥20%.

tent with the ability to span a membrane. These structures show significantly different amide mode frequencies (see Table XI). In particular, in the amide I region the differing predicted patterns of infrared modes and their splittings together with frequencies of intense Raman modes provide a strong basis for distinguishing between the various single- and double-stranded β-helices. Similar differences are calculated for amide III and amide V modes.

These calculated frequency patterns can form the basis for assigning structures to GA in various physical states from observed infrared and Raman spectra. This is done in the following paper (Naik and Krimm, 1986).

We are indebted to D. W. Urry and B. Lotz for providing us with coordinates for some of the structures.

This research was supported by National Science Foundation grants PCM-8214064 and DMR-8303610. One of us (Vaman M. Naik) wishes to acknowledge fellowship support from the Macromolecular Research Center at the University of Michigan.

Received for publication 19 July 1985 and in final form 10 December 1985.

REFERENCES

Abe, Y., and S. Krimm. 1972. Normal vibrations of crystalline polyglycine I. *Biopolymers.* 11:1817–1839.

Appel, H.-J., H. Bamberg, H. Alpes, and P. Läuger. 1977. Formation of ion channels by a negatively charged analog of gramicidin A. *J. Membr. Biol.* 31:171–188.

Arseniev, A. S., V. F. Bystrov, V. T. Ivanov, and Yu. A. Ovchinnikov. 1984. NMR solution conformation of gramicidin A. *FEBS (Fed. Eur. Biochem. Soc.) Lett.* 165:51–56.

Bamberg, E., and P. Läuger. 1973. Channel formation kinetics of gramicidin A in lipid bilayer membranes. *J. Membr. Biol.* 11:177–194.

Benedetti, E., B. DiBlasio, C. Pedone, G. P. Lorenzi, L. Tomasic, and V. Gramlich. 1979. A double stranded β-helix with antiparallel chains in a crystalline state and in chloroform. *Nature (Lond.).* 282:630.

Cheam, T. C., and S. Krimm. 1984. Transition dipole interaction in polypeptides: Ab initio calculation of transition dipole parameters. *Chem. Phys. Lett.* 107:613–616.

Cheam, T. C., and S. Krimm. 1985. Infrared intensities of amide modes in N-methylacetamide and poly(glycine I) from ab initio calculations of dipole moment derivatives of N-methylacetamide. *J. Chem. Phys.* 82:1631–1641.

Colonna-Cesari, F., S. Premilat, F. Heitz, G. Spach, and B. Lotz. 1977. Helical structures of poly(D-L-peptides). A conformational energy analysis. *Macromolecules.* 10:1284–1288.

Dwivedi, A. M., and S. Krimm. 1982*a*. Vibrational analysis of peptides, polypeptides, and proteins. XI. β-Poly(L-alanine) and its *N*-deuterated derivative. *Macromolecules.* 15:186–193; 1983. ibid 16:340.

Dwivedi, A. M., and S. Krimm. 1982*b*. Vibrational analysis of peptides, polypeptides, and proteins. X. Poly(glycine I) and its isotopic derivatives. *Macromolecules.* 15:177–185.

Dwivedi, A. M., and S. Krimm. 1984*a*. Vibrational analysis of peptides, polypeptides and proteins. 19. Force fields for α-helix and β-sheet structures in a side-chain point-mass approximation. *J. Phys. Chem.* 88:620–627.

Dwivedi, A. M., and S. Krimm. 1984*b*. Vibrational analysis of peptides, polypeptides, and proteins. XVIII. Conformational sensitivity of the α-helix spectrum: α_I- and α_{II}-poly(L-alanine). *Biopolymers.* 23:923–943.

Haydon, D. A., and S. B. Hladky. 1972. Ion transport across thin lipid membranes: a critical discussion of mechanisms in selected systems. *Q. Rev. Biophys.* 5:187–282.

Heitz, F., B. Lotz, and G. Spach. 1975. α_{DL} and π_{DL} helices of alternating poly-γ-benzyl-D-L-glutamate. *J. Mol. Biol.* 92:1–13.

Hesselink, F. T., and H. A. Scheraga. 1972. On the possible existence of α-helical structures of regular-sequence D,L copolymers of amino acids. Conformational energy calculations. *Macromolecules.* 5:455–463.

Iqbal, Z., and E. Weidekamm. 1979. Infrared spectroscopy of biomembrane channel: gramicidin A. *Infrared Phys.* 19:475–479.

Iqbal, Z., and E. Weidkamm. 1980. Raman and infrared spectroscopic study of gramicidin A conformations. *Arch. Biochem. Biophys.* 202:639–649.

Koeppe, II, R. E., and B. P. Schoenborn. 1984. 5-Å Fourier map of gramicidin A phased by deuterium-hydrogen solvent difference neutron diffraction. *Biophys. J.* 45:503–507.

Koeppe, II., R. E., K. O. Hodgson, and L. Stryer. 1978. Helical channels in crystals of gramicidin A and a cesium-gramicidin A complex: an x-ray diffraction study. *J. Mol. Biol.* 121:41–54.

Koeppe, II, R. E., J. M. Berg, K. O. Hodgson, and L. Stryer. 1979. Gramicidin A crystals contain two cation binding sites per channel. *Nature (Lond.).* 279:723–725.

Kolb, H. A., P. Läuger, and E. Bamberg. 1975. Correlation analysis of electrical noise in lipid bilayer membranes: kinetics of gramicidin A channel. *J. Membr. Biol.* 20:133–154.

Krasne, S., G. Eisenman, and G. Szabo. 1971. Freezing and melting of lipid bilayers and the mode of action of nonactin, valinomycin and gramicidin. *Science (Wash. DC).* 174:412–415.

Krimm, S. 1983. Vibrational analysis of conformation in peptides, polypeptides, and proteins. *Biopolymers.* 22:217–225.

Krimm, S., and Y. Abe. 1972. Intermolecular interaction effects in the amide I vibrations of β-polypeptides. *Proc. Natl. Acad. Sci. USA.* 69:2788–2792.

Lotz, B., F. Colonna-Cesari, F. Heitz, and G. Spach. 1976. A family of double helices of alternating poly(γ-benzyl-D-L-glutamate), a stereochemical model for gramicidin A. *J. Mol. Biol.* 106:915–942.

Moore, W. H., and S. Krimm. 1975. Transition dipole coupling in amide I modes of β-polypeptides. *Proc. Natl. Acad. Sci. USA.* 72:4933–4935.

Moore, W. H., and S. Krimm. 1976. Vibrational analysis of peptides, polypeptides, and proteins. I. Polyglycine I. *Biopolymers.* 15:2439–2464.

Nabedryk, E., M. P. Gingold, and J. Breton. 1982. Orientation of gramicidin A transmembrane channel. Infrared dichroism study of gramicidin in vesicles. *Biophys. J.* 38:243–249.

Naik, V. M. 1984. A vibrational analysis of LD-peptides. Ph.D. thesis. University of Michigan, Ann Arbor, MI.

Naik, V. M., and S. Krimm. 1984*a*. Vibrational analysis of the structure of crystalline gramicidin A. *Biophys. J.* 45:109–112.

Naik, V. M., and S. Krimm. 1984*b*. The structure of crystalline and membrane-bound gramicidin A by vibrational analysis. *Biochem. Biophys. Res. Commun.* 125:919–925.

Naik, V. M., and S. Krimm. 1984*c*. Vibrational analysis of peptides, polypeptides, and proteins. XVII. Normal modes of crystalline Pro-Leu-Gly-NH_2, a type II β-turn. *Int. J. Pept. Protein Res.* 23:1–24.

Naik, V. M., and S. Krimm. 1986. Vibrational analysis of the structure of gramicidin A. II. Vibrational spectra. *Biophys. J.* 49:1147–1154.

Naik, V. M., S. Krimm, J. B. Denton, G. Némethy, and H. A. Scheraga. 1984. Vibrational analysis of peptides, polypeptides, and proteins. XXVII. Structure of gramicidin S from normal mode analyses of low-energy conformations. *Int. J. Pept. Protein Res.* 23:613–626.

Ovchinnikov, Yu. A., and V. T. Ivanov. 1982. Helical structures of gramicidin A and their role in ion channeling. *In* Conformation in Biology. R. Srinivasan and R. H. Sarma, editors. Adenine Press, New York. 155–174.

Popov, E. M., and G. M. Lipkind. 1979. Conformation and mechanism of functioning of gramicidin A. *Mol. Biol. (Mosc.).* 13:363–376.

Prasad, B. V. V., and R. Chandrasekaran. 1977. Conformation of polypeptide chains containing both L- and D-residues. II. Double-

helical structures of poly-LD-peptides. *Int. J. Pept. Protein Res.* 10:129–138.

Ramachandran, G. N., and R. Chandrasekharan. 1972. Conformation of peptide chains containing both L- and D-residues. Part I. Helical structures with alternating L- and D-residues with special reference to the LD-ribbon and the LD-helices. *Indian J. Biochem. Biophys.* 9:1–11.

Rothschild, K. J., and H. E. Stanley. 1974. Raman spectroscopic investigation of gramicidin A′ conformations. *Science (Wash. DC).* 85:616–618.

Sengupta, P. K., and S. Krimm. 1985. Vibrational analysis of peptides, polypeptides, and proteins. XXXII. α-poly(L-glutamic acid). *Biopolymers.* 24:1479–1491.

Sychev, S. V., N. A. Nevskaya, S. T. Jordanov, E. N. Shephel, A. I. Miroshnikov, and V. T. Ivanov. 1980. The solution conformations of gramicidin A and its analogs. *Bioorg. Chem.* 9:121–151.

Sychev, S. V., and V. T. Ivanov. 1982. Conformational states of gramicidin A in solution and in the membrane. *In* Membranes and Transport. A. N. Martonosi, editor. Plenum Publishing Corp., New York. 2:301–307.

Urry, D. W. 1971. The gramicidin A transmembrane channel. A proposed π(L,D) helix. *Proc. Natl. Acad. Sci. USA.* 68:672–676.

Urry, D. W. 1972. A molecular theory of ion conducting channels: field dependent transition between conducting and nonconducting conformations. *Proc. Natl. Acad. Sci. USA.* 69:1610–1614.

Urry, D. W., M. C. Goodall, J. D. Glickson, and D. F. Mayers. 1971. The gramicidin A transmembrane channel. Characteristics of head-to-head dimerized π(L,D) helices. *Proc. Natl. Acad. Sci. USA.* 68:1907–1911.

Urry, D. W., A. Spisni, and Md. A. Khaled. 1979. Characterization of micellar-packed gramicidin A channels. *Biochem. Biophys. Res. Commun.* 88:940–949.

Urry, D. W., T. L. Trapane, and K. U. Prasad. 1983*a*. Is the gramicidin A transmembrane channel single-stranded or double-stranded helix? A simple unequivocal determination. *Science (Wash. DC).* 221:1064–1067.

Urry, D. W., R. G. Shaw, T. L. Trapane, and K. U. Prasad. 1983*b*. Infrared spectra of the gramicidin A transmembrane channel: the single stranded β^6-helix. *Biochem. Biophys. Res. Commun.* 114:373–379.

Veatch, W. R., E. T. Fossel, and E. R. Blout. 1974. The conformation of gramicidin A. *Biochemistry.* 13:5249–5256.

Veatch, W. R., R. Mathies, M. Eisenberg, and L. Stryer. 1975. Simultaneous fluorescence and conductance studies of planar bilayer membranes containing a highly active and fluorescent analogue of gramicidin A. *J. Mol. Biol.* 99:75–92.

Veatch, W., and L. Stryer. 1977. The dimeric nature of the gramicidin A transmembrane channel: conductance and fluorescence energy transfer studies of hybrid channels. *J. Mol. Biol.* 113:89–102.

Venkatachalam, C. M., and D. W. Urry. 1983. Theoretical conformational analysis of gramicidin A transmembrane channel. I. Helix sense and energetics of head-to-head dimerization. *J. Comput. Chem.* 4:461–469.

Wallace, B. A. 1983. Gramicidin A adopts distinctly different conformations in membranes and in organic solvents. *Biopolymers.* 22:397–402.

Wallace, B. A. 1984. Ion bound forms of the gramicidin A transmembrane channel. *Biophys. J.* 45:114–116.

Wallace, B. A., W. R. Veatch, and E. R. Blout. 1981. Conformation of gramicidin A in phospholipid vesicles: circular dichroism studies of the effects of ion binding, chemical modifications and lipid structure. *Biochemistry.* 20:5754–5760.

Weinstein, S., B. A. Wallace, E. R. Blout, J. Morrow, and W. Veatch. 1979. Conformation of gramicidin A channel in phospholipid vesicles: a ^{13}C and ^{19}F nuclear magnetic resonance study. *Proc. Natl. Acad. Sci. USA.* 76:4230–4234.

Weinstein, S., B. A. Wallace, J. S. Morrow, and W. R. Veatch. 1980. Conformation of the gramicidin A transmembrane channel: a ^{13}C-NMR study of ^{13}C-enriched gramicidin in phosphatidylcholine vesicles. *J. Mol. Biol.* 143:1–19.

Zingsheim, H. P., and E. Neher. 1974. The equivalence of fluctuation analysis and chemical relaxation measurements: a kinetic study of ion pure formation in thin lipid membranes. *Biophys. Chem.* 2:197–207.